Sensing and Bio-Sensing Research 11 (2016) 78–85

Contents lists available at ScienceDirect

Sensing and Bio-Sensing Research

journal homepage: www.elsevier.com/locate/sbsr

Soft-film dynamics of SH-SAW sensors in viscous and viscoelastic fluids

A. Vikström *, M.V. Voinova

Department of Physics, Chalmers University of Technology, Kemigården 1, 412 96 Göteborg, Sweden

ARTICLE INFO

Article history:
Received 7 June 2016
Received in revised form 16 August 2016
Accepted 22 August 2016

Keywords:
Acoustic sensor
Surface acoustic wave
SH-SAW sensor
Viscoelasticity
Sensor modeling

ABSTRACT

We theoretically investigate surface acoustic waves with horizontal polarization (SH-SAWs) propagating in a three-layer system consisting of an elastic substrate and two viscoelastic overlayers. For the limiting case of an acoustically thin middle layer and an infinite top layer, we derive analytical expressions for the phase velocity shift and the wave attenuation. These expressions demonstrate the importance of taking into account the viscoelastic coupling between the two overlayers. Numerical calculations using a combined Maxwell/Voigt scheme confirm our analytical results and also indicate that it is possible for viscoelasticity to cause SH-SAWs to vanish.

1. Introduction

The dynamics of soft polymeric and biological materials can be characterized by measuring their viscoelastic response to oscillatory stress [1]. This is the underlying principle of acoustic sensors in soft-matter applications, which broadly can be categorized into those using bulk acoustic waves (e.g. a quartz crystal microbalance, or QCM) and those using surface acoustic waves (SAW) (for a review, see e.g., refs. [2–5]).

SAW sensors are beneficial in many applications due to their higher operational frequencies enabling an increased sensitivity [6–9]. For sensor applications in liquids, which is typical for biological applications, SAW sensors usually use shear-horizontal surface acoustic waves (SH-SAW), since out-of-surface vibrations result in large viscous losses [10].

Since the utility of SH-SAW sensors in liquids was first reported in the 90s [10,11], these devices have become increasingly used for in situ characterization of biomolecular layers [12,13] and enabled probing of the masses and material properties of biological layers formed by adsorption of e.g., proteins, lipid vesicles, and cells, from a bulk solution onto the sensing surface [14,15,5]. Both QCM [16] and SAW [14] experiments show that these biological layers cannot be considered as rigid films, but must rather be treated as viscoelastic. Also, an alteration in physical parameters (e.g., temperature, water content, interaction energy with the substrate) or addition of chemical compounds (e.g., lipids [13], peptides [16]) may significantly influence the softness of these layers.

In a typical SH-SAW sensor experiment, the phase velocity shift and the wave attenuation due to the presence of overlayers on the sensing surface is measured [5,17]. By comparing with theory, these quantities can then be related to e.g., deposited surface mass and viscoelastic parameters. As has been learned from studies of the QCM [18,19], many standard assumptions for the system response break down when considering soft (viscoelastic) materials, e.g., for a QCM operated in a liquid environment there is a deviation [19] from the linear mass response predicted by the Sauerbrey relation [20] and the Kanazawa-Gordon term for viscous loading [21]. Theoretical work is thus vital for a correct interpretation of sensor data, and is typically based on a continuum mechanics treatment of multilayer structures [22,23], composed of elastic [24], viscous [25,26] or viscoelastic materials.

In a recent paper by Liu [27], the wave attenuation and mass sensitivity of a SH-SAW sensor was derived from a model comprised of a viscoelastic guiding layer (described by the Maxwell-Weichert model) on top of a piezoelectric elastic substrate. Oh et al. [28] studied a model with a viscoelastic guiding layer sandwiched between two rigid layers, resting on top of an elastic substrate. They then derived expressions for the sensor-optimized layer thicknesses. A model with three to four viscoelastic layers (described by the Maxwell model) resting on an elastic substrate was studied by McHale, Newton, and Martin [29]. They derived the dispersion equation for arbitrary layer thicknesses and analyzed it for the purpose of deriving the mass sensitivity from the dispersion curve. However, the authors did not consider the effect of viscoelastic coupling between the overlayers.

Here, we study the propagation of SH-SAWs in a system consisting of two viscoelastic layers on the surface of an elastic substrate. We demonstrate the effect of viscoelastic coupling on the phase velocity shift and the wave attenuation and show that this effect cannot be neglected when interpreting SH-SAW sensor data for soft layers in liquid-phase environments — a situation typical of biosensors. We also use our model to analyze glycerol/water mixtures, which have been used in

* Corresponding author.
E-mail address: anton.vikstrom@chalmers.se (A. Vikström).

http://dx.doi.org/10.1016/j.sbsr.2016.08.004

the calibration of biosensors [14]. Finally, we consider estimation of the viscoelastic parameters of a soft film from SH-SAW sensor data, with particular emphasis on the disentanglement of the elasticity and the viscosity.

In Section 2 we derive the general dispersion equation of this system. In Section 3.1 we then give analytical expressions for the phase velocity shift and attenuation for the limiting case of a thin film oscillating in a bulk liquid. These expressions could be used for mass and parameter estimation from experimental measurements. We then analyze numerical solutions for the phase velocity shift and attenuation in Section 3.2 using a combined Maxwell and Voigt scheme.

2. Model

We consider a three-layer system consisting of an elastic solid substrate (index 0), a viscoelastic middle layer (index 1) and a viscoelastic top layer (index 2), see Fig. 1. The solid substrate occupies the negative half-space $z < 0$ The middle layer rests on top of the substrate and has thickness h. On top of that rests the top layer, which has thickness Δh. We will use continuum mechanics to derive a general solution for a SH-SAW propagating on the surface of the solid substrate, in the interface between the substrate and the middle layer ($z = 0$). The displacement field of the SH-SAW penetrates into the middle and top layers, requiring a matching of solutions at the boundaries. The SH-SAW is taken to propagate in the y-direction, with shear displacement in the x-direction (Fig. 1).

In the solid substrate (index 0), the displacement field of a SH-SAW (which involves no compression) is given by the transverse wave equation [30]:

$$\partial_t^2 \vec{u}_0 = v_0^2 \Delta \vec{u}_0, \quad v_0 = \sqrt{\frac{\mu_0}{\rho_0}}, \tag{1}$$

where we have defined the speed of sound in the substrate, v_0, in terms of the substrate elastic shear modulus μ_0 and mass density ρ_0. When we consider a plane wave in the y-direction ($\propto \exp(-iky + i\omega t)$), with displacement in x-direction only, $\vec{u}_0 = (u_0, 0, 0)$, and note that, due to symmetry, the displacement should be independent of x, $u_0 = u_0(y,z)$, we find that

$$u_0 = A_0 e^{\varkappa z} e^{-iky + i\omega t}, \tag{2}$$

where we kept only the solution which decays into the solid (negative z-direction). A_0 is an amplitude, not specified by the theory. We have

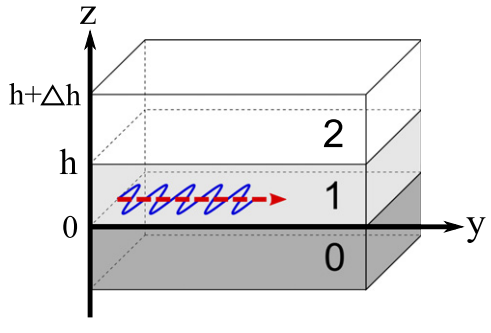

Fig. 1. The system geometry. The considered three-layer system. The substrate (index 0) is an elastic solid, whereas the middle (index 1) and top (index 2) layers are viscoelastic. The boundaries between the layers are at $z = 0$ and $z = h$, with a free top surface at $z = h + \Delta h$. On the substrate surface, $z = 0$, a SH-SAW propagates with wavevector in the y-direction (dashed red arrow) and displacement in the x-direction (blue sinusoidal line, x is directed out from the paper). Each layer covers the entire xy-plane.

defined

$$\varkappa = \sqrt{k^2 - \frac{\omega^2}{v_0^2}}, \quad \varkappa > 0, \tag{3}$$

which is the wavevector z-component times the imaginary unit. The real part of $\varkappa$ is the inverse penetration depth into the bulk substrate.

We will now consider SH-SAW solutions in the middle (index 1) and top (index 2) viscoelastic layers. The viscoelasticity of the two layers can be modeled by complex shear moduli [1] μ_i^*, $i = 1,2$, where the asterisk indicates that the shear modulus is complex. The equation of motion for a SH-SAW is then simply the transverse wave equation, Eq. (1), same as in the substrate but with a complex modulus $\mu_i^{(*)}$, and the displacement field of a SH-SAW is found in an analogous way. However, due to the finite extent of the layer in the z-direction, we must now keep both solutions. We find

$$u_i = A_0 \left(A_i e^{\xi_i z} + B_i e^{-\xi_i z} \right) e^{-iky + i\omega t}, \quad i = 1,2, \tag{4}$$

where A_0 has been factored out for convenience, and

$$\xi_i = \sqrt{k^2 - \omega^2 \frac{\rho_i}{\mu_i^*}}, \quad i = 1,2, \tag{5}$$

where ρ_i is the mass density of layer i.

Eqs. (2), (3), (4), and (5), give the general solutions for a SH-SAW in each of the three layers. Suitable boundary conditions must now be used to relate solutions in different layers to each other. We will adopt the no-slip boundary condition, meaning that both the velocity of the displacement and the viscoelastic stress should vary continuously across layer boundaries. At the interfaces between media, at $z = 0$ and $z = h$, we thus require that the velocities in the two media should be equal,

$$\partial_t u_0 \big|_{z=0} = \partial_t u_1 \big|_{z=0}, \tag{6}$$

$$\partial_t u_1 \big|_{z=h} = \partial_t u_2 \big|_{z=h}.$$

This gives us two equations for the coefficients:

$$A_1 + B_1 = 1, \tag{7}$$

$$A_1 e^{\xi_1 h} + B_1 e^{-\xi_1 h} = A_2 e^{\xi_2 h} + B_2 e^{-\xi_2 h}. \tag{8}$$

At the same two interfaces we also require that, for a normal vector $\vec{n}$ directed into one of the media (i.e. away from the other),

$$n_k \sigma_{jk}^{(0)} \big|_{z=0} = n_k \sigma_{jk}^{(1)} \big|_{z=0}, \tag{9}$$

$$n_k \sigma_{jk}^{(1)} \big|_{z=h} = n_k \sigma_{jk}^{(2)} \big|_{z=h},$$

where $\sigma_{jk}^{(i)}$ is the stress tensor in layer i. Since we have $\vec{n} = (0,0,1)$ and, for a SH-SAW ($\sigma_{ij} = 0$), the stress tensor is given by [30]

$$\sigma_{jk}^{(i)} = 2\mu_i^* u_{jk}^{(i)}, \tag{10}$$

where $u_{jk}^{(i)}$ is the corresponding strain tensor, we get, using Eqs. (2) and (4),

$$\mu_1^* \xi_1 (A_1 - B_1) = \mu_0 \varkappa, \tag{11}$$

$$\frac{\mu_1^* \xi_1}{\mu_2^* \xi_2} \left(A_1 e^{\xi_1 h} - B_1 e^{-\xi_1 h} \right) = A_2 e^{\xi_2 h} - B_1 e^{-\xi_2 h}. \tag{12}$$

At the free top surface at $z = h + \Delta h$ we have zero stress. From this, using Eqs. (10) and (4), we get

$$A_2 e^{\xi_2(h+\Delta h)} = B_2 e^{-\xi_2(h+\Delta h)}. \tag{13}$$

Eqs. (7), (8), (11), (12), and (13) are five equations for five unknown coefficients A_1, A_2, B_1, B_2 and $\varkappa$ (the amplitude of the substrate SAW, A_0, is a parameter). Solving these equations for $\varkappa$ leads to

$$\varkappa = \frac{\mu_1^* \xi_1}{\mu_0} \frac{F_- - e^{2\xi_1 h} F_+}{F_- + e^{2\xi_1 h} F_+}, \tag{14}$$

where we have defined

$$F_\pm = \mu_1^* \xi_1 \pm \mu_2^* \xi_2 \tanh(\Delta h \xi_2). \tag{15}$$

Since $\varkappa, \xi_1$ and ξ_2 all depend on k and ω (see Eqs. (3) and (5), Eq. (14) is an implicit dispersion equation for the SH-SAW. By substituting ξ_1, ξ_2, and k with $\varkappa$, it becomes an equation for $\varkappa$, which is the variable we solve for. In Section 3.1, we relate the solution $\varkappa$ to measurable characteristics, specifically the phase velocity shift and the attenuation.

3. Results and discussion

3.1. Phase velocity shift and attenuation

The dispersion Eq. (14) can, in the long-wavelength approximation, be related to measureable characteristics of the system. These characteristics are the phase velocity shift $\Delta v / v_0$ (relative to the speed of shear waves in the bulk substrate, $v_0 \to v_0 + \Delta v$) and the attenuation coefficient Γ (the wave decays exponentially during propagation, $u \propto \exp(-\Gamma y)$). The phase velocity shift of a long-wavelength SH-SAW is given by

$$\frac{\Delta v}{v_0} \approx -\mathrm{Re}\left(\frac{\varkappa^2}{2(\omega/v_0)^2}\right) \tag{16}$$

and the attenuation coefficient (scaled by the wavevector k) is given by

$$\frac{\Gamma}{k} \approx -\mathrm{Im}\left(\frac{\varkappa^2}{2(\omega/v_0)^2}\right), \tag{17}$$

where $\varkappa$ is the solution to the dispersion Eq. (14). The complex shear modulus of each viscoelastic medium consists of a storage modulus (the real part) and a loss modulus (the imaginary part). We write

$$\mu_1^* = g' + ig'',$$

$$\mu_2^* = G' + iG'', \tag{18}$$

where g' and G' (g'' and G'') are the storage (loss) moduli of the middle and top layer, respectively.

In order to arrive at analytical expressions for the phase velocity shift and attenuation coefficient, we consider the limiting case of an acoustically thin middle layer in a bulk (semi-infinite) top layer. For a bulk top layer, Eq. (15) is simplified:

$$\xi_2 \Delta h \to \infty, \quad F_\pm \to \mu_1^* \xi_1 \pm \mu_2^* \xi_2. \tag{19}$$

(In taking this limit, we assumed that $\mathrm{Re}(\xi_2 \Delta h) > 0$.) For a thin õmiddle layer, we can expand in the small parameter $\xi_1 h \ll 1$. We then find that, to linear order, the phase velocity shift is given by

$$\frac{\Delta v}{v_0} \approx \frac{v_0^2}{2\mu_0^2} \left\{ \rho_2 G' + \left(G''^2 - G'^2\right) \frac{1}{v_0^2} + [h\rho_1]\rho_2 \left(G' K_1 - G'' K_2\right) \right\} \tag{20}$$

and the attenuation coefficient is given by

$$\frac{\Gamma}{k} \approx \frac{v_0^2 \rho_2}{2\mu_0^2} \left\{ G'' - \frac{2G'G''}{\rho_2 v_0^2} + [h\rho_1]\left(G'' K_1 + G' K_2\right) \right\}, \tag{21}$$

where we have enclosed the middle layer surface mass density $[h\rho_1]$ in brackets for emphasis, since it is of primary importance in sensor applications. Here we have defined

$$K_1 = -\omega \sqrt{\frac{2}{\rho_2}} \left\{ \frac{G'\gamma_- - G''\gamma_+}{G'^2 + G''^2} + \frac{\rho_2}{\rho_1} \frac{\left(g'G' + g''G''\right)\gamma_- - \left(g'G'' - g''G'\right)\gamma_+}{\left(g'^2 + g''^2\right)\sqrt{G'^2 + G''^2}} \right\}, \tag{22}$$

$$K_2 = \omega \sqrt{\frac{2}{\rho_2}} \left\{ \frac{G''\gamma_- + G'\gamma_+}{G'^2 + G''^2} - \frac{\rho_2}{\rho_1} \frac{\left(g'G' + g''G''\right)\gamma_+ + \left(g'G'' - g''G'\right)\gamma_-}{\left(g'^2 + g''^2\right)\sqrt{G'^2 + G''^2}} \right\},$$

where

$$\gamma_\pm = \sqrt{\sqrt{G'^2 + G''^2} \pm G'}. \tag{23}$$

Both the phase velocity shift (Eq. (20)) and the attenuation coefficient (Eq. (21)) contain a contribution from the viscoelasticity of the bulk top layer which does not depend on the middle layer surface mass density $[h\rho_1]$, a "bulk term". The coefficient of the surface mass density, the mass sensitivity, depends on a combination of the viscoelastic parameters for both overlayers. Not taking this viscoelastic coupling is into account would lead to e.g., an erroneous estimate of the deposited surface mass.

If we consider the special case of a Newtonian liquid top layer, $G' = 0$, $G'' = \eta_2 \omega$, we recover the results of ref. [31], Eqs. (8) and (9), plus an additional bulk term in the velocity shift, $\eta_2^2 \omega^2 / (2\mu_0^2)$, which for reasonable SAW working frequencies (~100 MHz) in water (or liquids of comparable viscosity) is negligible ($\sim 10^{-10}$). In the case of higher frequencies and/or more viscous liquids however, this bulk term becomes significant, as will be seen in Section 3.2.

The assumption of a thin middle layer, under which Eqs. (20) and (21) were derived, is equivalent to a layer thickness satisfying $h \ll |\mathrm{Re}(1/\xi_1)|$ and $h \ll |\mathrm{Im}(1/\xi_1)|$. Contour plots of the real and imaginary parts of ξ_1, for a range of middle layer parameters are given in Fig. 2, for the frequency $f = 100$ MHz and film mass density $\rho = 1.0$ g/cm^3.

3.2. Numerical analysis using a Voigt-Maxwell scheme

To study the influence of the viscoelastic coupling in the system, we performed numerical calculations using viscoelastic parameters taken from experiments. We plot the shift in phase velocity $\Delta v / v_0$ and the scaled attenuation coefficient Γ / k against middle layer (film) thickness h for various systems and two different frequencies, with the top taken as a bulk medium ($\Delta h \to \infty$). For substrate parameters, we used quartz values, $\mu_0 = C_{44} = 58$ GPa and mass density $\rho_0 = 2.6$ g/cm^3 [32]. Viscoelastic moduli are, in general, frequency dependent. For our analysis, we simply employed two simple and well-known models for this dependence. The middle layer was chosen as either a rigid (elastic) polymer film or as a soft polymer film modeled as a *Voigt material* (viscoelastic solid), whereas the top bulk layer was chosen as either a Newtonian fluid or as a *Maxwell material* (viscoelastic fluid), see Fig. 3.

A Voigt material is a material described by the Voigt model of viscoelasticity, which can be represented by a spring (elasticity element) and a dashpot (viscosity element) connected in parallel; the total strain and stress is thus given by the sum of that of the spring and the dashpot.

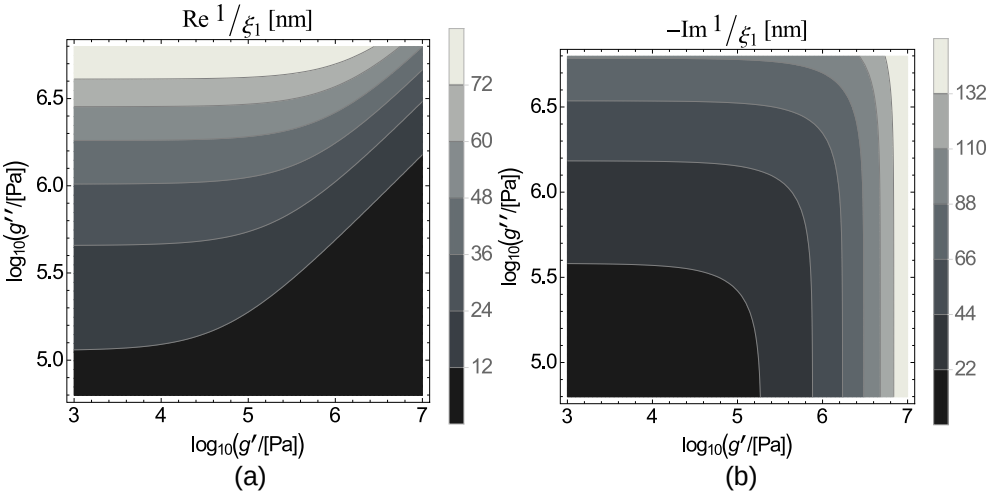

Fig. 2. Thin-film condition. The real (a) and negative imaginary (b) parts of $1/\xi_1$ (in nm), for $f = 100$ MHz. The validity of the expansions (20) and (21) amounts to the film thickness $h \ll 1/\xi_1$.

Using this model, the storage and loss moduli of the film (middle layer) are given by

$$g' = \mu_1, \quad g'' = \eta_1 \omega. \tag{24}$$

For low frequencies, a Voigt material behaves as an elastic solid, but it becomes more viscous and less elastic as the frequency increases. In the limit of infinite frequency, it behaves as a viscous liquid [33].

In contrast, the Maxwell model of viscoelasticity is represented by a spring and a dashpot element connected in series. The stress in each component is then equal to the total stress. When this model is used for the bulk top layer, its storage and loss moduli are given by

$$G' = \frac{\mu_\infty}{1 + \left(\frac{\mu_\infty}{\eta_2 \omega}\right)^2}, 4G'' = \frac{\eta_2 \omega}{1 + \left(\frac{\eta_2 \omega}{\mu_\infty}\right)^2}. \tag{25}$$

For low frequencies, a Maxwell material behaves as a viscous liquid, but as the frequency increases it becomes increasingly elastic. The parameter μ_∞ is the acquired shear modulus in the limit of infinite frequency. A Voigt (Maxwell) material is sometimes referred to as a "viscoelastic solid (fluid)", due to its behavior at low frequencies [33].

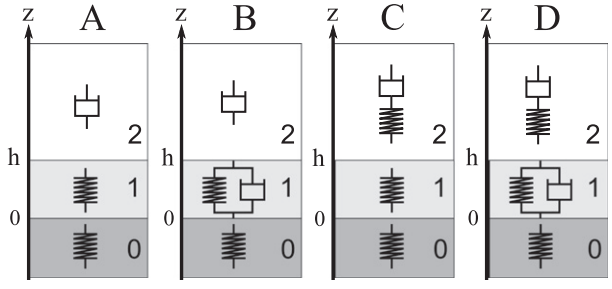

Fig. 3. Viscoelasticity schemes. Four different schemes for the three-layer system. In each scheme, the substrate (index 0) is modeled as an elastic solid (represented by a spring). In schemes A and C, the middle layer (index 1) is considered a rigid film, also an elastic solid (spring). In scheme A, the rigid film oscillates in a viscous top fluid (Newtonian, represented by a dashpot), whereas in scheme C the top fluid is a viscoelastic fluid, as described by the Maxwell model (spring and dashpot in series). In schemes B and D, the middle layer is a soft film whose viscoelasticity is described by the Voigt model (spring and dashpot in parallel). In scheme B, the soft film oscillates in a viscous top fluid (Newtonian, represented by a dashpot), whereas in scheme D the top fluid is a viscoelastic fluid, described by the Maxwell model (spring and dashpot in series).

3.2.1. Soft and rigid films in viscous liquids

The rigid polymer film material is taken as PMMA, described by an elastic shear (storage) modulus $g' = \mu_1 = 0.15$ MPa, and a mass density of 1.2 g/cm^3 [34]. For the soft polymer film, material parameters for PLL-PGA were adopted from [35]. In that experimental work, the shear modulus $g' = \mu_1 = 0.15$ MPa and the shear viscosity $\eta_1 = g''/\omega = 3.4$ cP were extracted from QCM-D measurements using the Voigt model. The mass density of PLL-PGA is 1.5 g/cm^3 The solutions corresponding to the rigid (soft) film are shown as solid (dashed) lines in Figs. 4 and 5.

The bulk top layer was either a Newtonian fluid (water, $\eta_2 = 0.89$ cP) or a Maxwell fluid — a 32.9% glycerol/water mixture (parameters taken from ref. [36] and shown in Table 1). For a relatively low glycerol concentration of 32.9% and frequencies up to 100 MHz, as used in Figs. 4 and 5, a glycerol-water mixture is essentially a Newtonian fluid ($G' << G''$). The main difference between water and the glycerol-water mixture is then the magnitude of the viscosity. For comparison with the two cases of viscous loading, we also present corresponding solutions for air as a top bulk layer (treated as a Newtonian fluid with low mass density and viscosity, $\rho_2 = 0.0012$g/cm^3, $\eta_2 = 0.018$ cP).

We considered two different dynamic regimes within range of SAW devices [3] — "low frequency" ($f = 5$ MHz) and "high frequency" ($f = 100$ MHz). The numerical results are shown as a family of curves in plots of the phase velocity shift $\Delta v / v_0$ and the scaled attenuation Γ / k. In Figs. 4 and 5., the curves corresponding to 32.9% glycerol are indicated with black squares (■), those corresponding to water with circles (○), and those corresponding to air are unmarked.

Figs. 4 and 5 reveal the important contributions of viscosity effects in the calculated SH-SAW characteristics. It is shown that the influence of

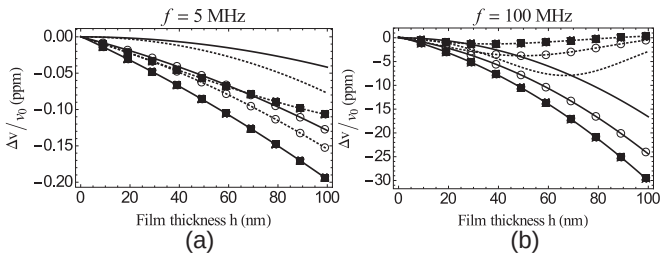

Fig. 4. Velocity shift for rigid and soft films. The shift in phase velocity (ppm) of a SH-SAW at two different frequencies, (a) 5 MHz and (b) 100 MHz, for a quartz substrate covered by a rigid (solid lines) or soft (dashed lines) polymer film. The films are loaded by different bulk fluids, as indicated by the markers: 32.9% glycerol in water (■), water (○), air (no markers).

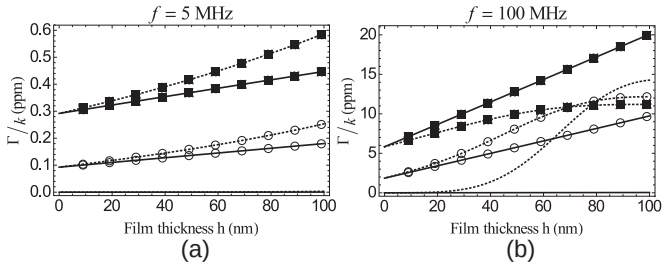

Fig. 5. Attenuation for rigid and soft films. The scaled attenuation coefficient (ppm) of a SH-SAW at two different frequencies, (a) 5 MHz and (b) 100 MHz, for a quartz substrate covered by a rigid (solid lines) or soft (dashed lines) polymer film. The films are loaded by different bulk fluids, as indicated by the markers: 32.9% glycerol in water (■), water (○), air (no markers).

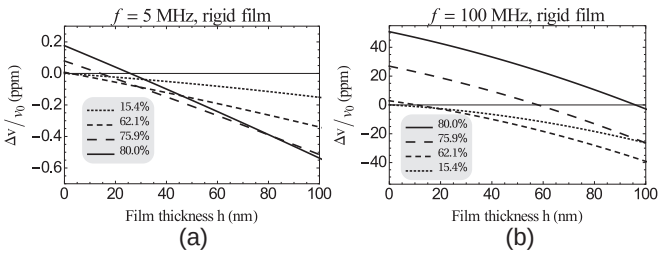

Fig. 6. Velocity shifts for a rigid film in glycerol/water mixtures. The shift in phase velocity (ppm) of a SH-SAW at two different frequencies, (a) 5 MHz and (b) 100 MHz, for a rigid film loaded by glycerol/water mixtures of different concentrations (see inset).

the top fluid viscosity is heavily dependent on the softness of the film. For a low viscosity top fluid, the phase velocity shift (Fig. 4) is different for rigid and soft polymer films. Comparing the curves for a rigid film (solid lines) in water (○) and a 32.9% glycerol/water solution (■), we see that the absolute value of the phase velocity shift $|\Delta v/v_0|$ increases with the top fluid viscosity η_2. On the other hand, comparing the corresponding curves (○ and ■) for the soft film (dashed lines), we observe that the absolute value of the velocity shift, $|\Delta v/v_0|$, is actually *smaller* for the more viscous top fluid (the glycerol-water mixture). In the linear regime, the change in slope with top fluid viscosity can be understood from the *h*-coefficient in Eq. (20). This shows that neglecting the interplay between the film softness and the top fluid when interpreting velocity shift measurements can lead to an underestimation of the film thickness, and thus also its mass. This effect is analogous to the reduction in the resonance frequency shift for a QCM-D due to viscous coupling between a soft film and a viscous top fluid [18]. That effect has been referred to as "the missing mass effect" [19]. Here, we have demonstrated a similar effect for SH-SAW sensors.

The soft-film plots (dashed lines) in Fig. 4b exhibit a turning point where the sign of the derivative of $\Delta v/v_0$ changes sign. This is a characteristic of soft films which has sometimes been called "tail-raising" [37,38] and has been confirmed experimentally [39]. In the case of a rigid film, there is no tail-raising; the phase velocity is initially close to that in the substrate (v_0) but, as the film thickness increases, the velocity undergoes a sharp decrease and eventually approaches that in the film (v_1) [40,4]. However, if the film is sufficiently soft (viscoelastic), the velocity does not undergo a sharp decrease from v_0 but instead shows tail-raising behavior, after which the velocity can even become larger than v_0 [39,4].

We now turn our attention to the attenuation coefficient (Fig. 5). For low frequency, Fig. 5a shows a monotonic growth of the (scaled) attenuation coefficient Γ/q with shear viscosity η_2 of the top Newtonian fluid. However, at high frequency (Fig. 4b), the curve corresponding to the soft film (dashed) in the glycerol-water mixture (■) has acquired a reduction in slope relative to the case of the soft film in water (○). Beyond a certain film thickness *h*, this curve drops below the curve corresponding to the case of pure water (dashed, ○), so an increased top fluid viscosity actually *decreases* the attenuation. This is contrary to the case of a rigid film, where a more viscous top fluid leads to more viscous losses and thus an increased attenuation. The analytical results (21), (22), and (23) confirm this interplay between the softness of the film and the viscosity of the top fluid.

Table 1
Parameter values used for glycerol/water mixtures. "Gl. conc." is the concentration of glycerol in water. The infinite-frequency shear modulus is $\mu_\infty = 50$ MPa. Values adopted from ref. [36].

Gl. conc	Viscosity η_2 (cP)	Density ρ_2 (g/cm^3)
0.4	1.4	1.017
0.9	2.7	1.038
0.1	10.2	1.075
0.9	33.2	1.093
0.0	49.5	1.098

3.2.2. Soft and rigid films in viscoelastic glycerol-water mixtures

We will now investigate the effect of glycerol/water mixtures of different concentrations, ranging from 15.4% to 80% glycerol, together with both a rigid and a soft film and for low and high frequency (as before). The glycerol/water mixtures are modeled as viscoelastic fluids, so (referring to Fig. 3) we are working in schemes C (rigid film) and D (soft film). Parameter values for the glycerol/water mixtures, were taken from ref. [36] and are given for reference in Table 1. Glycerol/water mixtures are of particular interest, since they have been used for calibration of biosensors [14].

By comparing Fig. 6a and b, we can see that the phase velocity shift for the case of a rigid film is qualitatively similar for both low and high frequency (although for high frequency, the curves are slightly nonlinear). Increasing the concentration of glycerol increases the negativity of the slope of $\Delta v/v_0$ as a function of film thickness *h*. This is essentially the well-known increase in mass sensitivity for SAW sensors when operated in a viscous liquid [31]. For low concentrations, the *h*-independent bulk term is negligible. However, as the glycerol concentration increases, the velocity shift changes sign since the growing *h*-independent bulk term increasingly dominates the thin-film deviation from v_0.

In contrast, for the case of the soft film, the plots of the velocity shift, Fig. 7, appear qualitatively different for low and high frequency. For both frequencies, the minimum velocity (lowest point in the plots) is attained for the lowest glycerol concentration, 15.4%. For this concentration, the $\Delta v / v_0$ curve has an initially negative slope but eventually reaches a turning point where the derivative changes sign. When the concentration of glycerol is increased, this turning point is shifted upwards and to the left in the plot. The shift upwards means that the phase velocity shift $\Delta v / v_0$ as well as the initial slope of the curve (the thin-film mass sensitivity) changes sign for some critical concentration of glycerol, approximately 60%, corresponding to $\eta_2 \approx 10$ cP. The shift to the left means that the turning point is reached for lower film thicknesses *h* for higher glycerol concentrations. It is apparent that both the

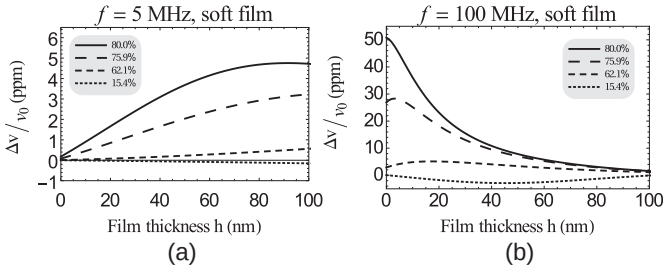

Fig. 7. Velocity shifts for a soft film in glycerol/water mixtures. The shift in phase velocity (ppm) of a SH-SAW at two different frequencies, (a) 5 MHz and (b) 100 MHz, for a soft film loaded by glycerol/water mixtures of different concentrations (see inset).

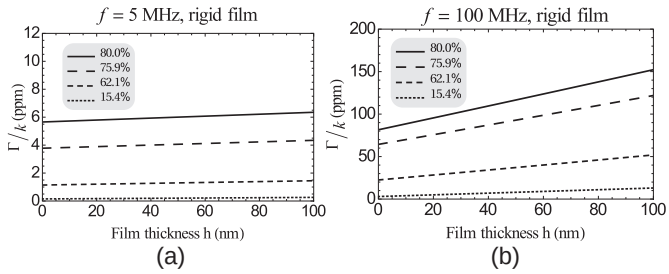

Fig. 8. Attenuation for a rigid film in glycerol/water mixtures. The scaled attenuation coefficient (ppm) of a SH-SAW at two different frequencies, (a) 5 MHz and (b) 100 MHz, for a rigid film loaded by glycerol/water mixtures of different concentrations (see inset).

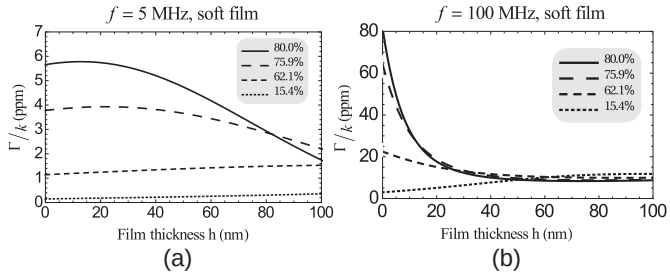

Fig. 9. Attenuation for a soft film in glycerol/water mixtures. The scaled attenuation coefficient (ppm) of a SH-SAW at two different frequencies, (a) 5 MHz and (b) 100 MHz, for a soft film loaded by glycerol/water mixtures of different concentrations (see inset).

magnitude and the sign of the phase velocity shift for a soft film in a glycerol-water mixture depend on frequency.

Analysis of the plots of the attenuation coefficient yields a similar pattern. For the rigid film (Fig. 8), the behavior is qualitatively similar for different frequencies; for increasing glycerol concentration, we observe a constant shift of the curves, corresponding to a bulk contribution, as well as an increase in the slope. For the soft film however (Fig. 9), we see slopes of both signs in the thin-film region.

3.2.3. Determining the viscoelastic parameters via measurement

Finally, we consider a soft film (Voigt model) of unknown material parameters μ_1 and η_1, with thickness $h = 5$ nm and mass density $\rho_1 = 0.8\text{g/cm}^3$. The parameter range is chosen such as to encompass the values known for lipid bilayers [16]. As a bulk top fluid, we consider water, a Newtonian liquid (scheme B, see Fig. 3). We consider only high frequency ($f = 100$ MHz). Contour plots of the phase velocity shift and the attenuation coefficient are shown in Fig. 10. One contour line from the velocity plot (dashed white line) is transposed onto the corresponding attenuation plot. A velocity measurement yielding a value corresponding to the dashed white line implies that the film parameters lie on this line in parameter space, but it alone cannot disentangle the film elasticity and viscosity. However, an attenuation measurement can resolve this ambiguity by finding the position on the dashed white line consistent with the measured attenuation. This demonstrates the need for simultaneous velocity and attenuation measurements when attempting to discern viscoelastic parameters.

The case depicted in Fig. 10 requires a very fine resolution of the measured characteristics (on the order of 0.1 ppm). To remedy this, we can replace the water with a fluid of higher viscosity, yielding a higher mass sensitivity. We thus consider the same variable soft film in high frequency, but replace the water with an 80.00% glycerol/water mixture, a Maxwellian fluid (scheme D see Fig. 3). (We choose this extreme for demonstrative purposes.) Contour plots are shown in Fig. 11. While the sensitivity has been increased, we observe that, for the given thickness and in large regions of film-parameter space, the real part of the solution to Eq. (14) becomes zero or even negative, Re $(\varkappa) \leq 0$, corresponding to a depth delocalization of the wave (see Eq. (2). This indicates that, for certain parameters, SH-SAW solutions cannot exist. We confirmed that this is not due to a violation of the Love condition, $v_1 < v_0$, but is in fact caused by viscoelasticity. It might be understood as the viscoelasticity creating effective boundary conditions on the substrate surface which are incompatible with SH-SAWs. Further calculations revealed that this vanishing of SH-SAW solutions appears only for viscoelastic films, with onset beyond a critical film thickness. This critical thickness can be very small, as can be seen from Fig. 11, for which $h = 5$ nm. As the film thickness h is increased, the support for SH-SAW solutions is periodically restored and destroyed in a repeating pattern reminiscent of the observed resonance patterns for acoustically thick elastic films [41]. This phenomenon, viscoelastic destruction of SH-SAW solutions, can appear even without any viscoelastic loading (no top layer). However, viscoelastic loading can significantly affect it, as shown by Figs. 10 and 11.

The possibility of a viscoelasticity-induced destruction of SH-SAWs must be taken into account when operating SH-SAW sensors with soft films, and could be an important consideration in biosensing experiments.

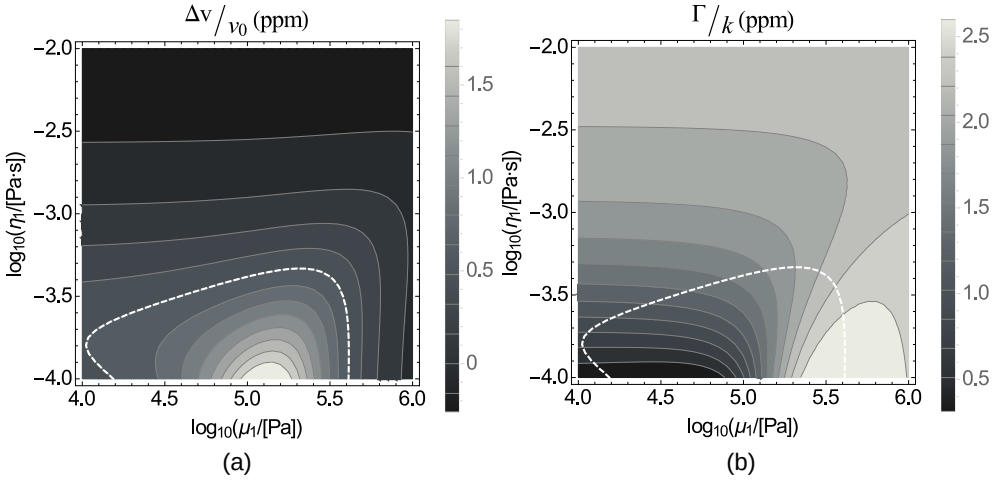

Fig. 10. Measurable characteristics for different film parameters with water loading. The phase velocity shift (a) and scaled attenuation (b) at 100 MHz for a viscoelastic solid film ($h = 5$ nm) of varying parameters μ_1 and η_1, loaded by bulk water, a Newtonian liquid (scheme C, see Fig. 3). One contour line (dashed white line) in the velocity shift plot (a) is also plotted in the attenuation plot (b). Intersecting contour lines indicate that the two viscoelastic parameters should be distinguishable via measurements.

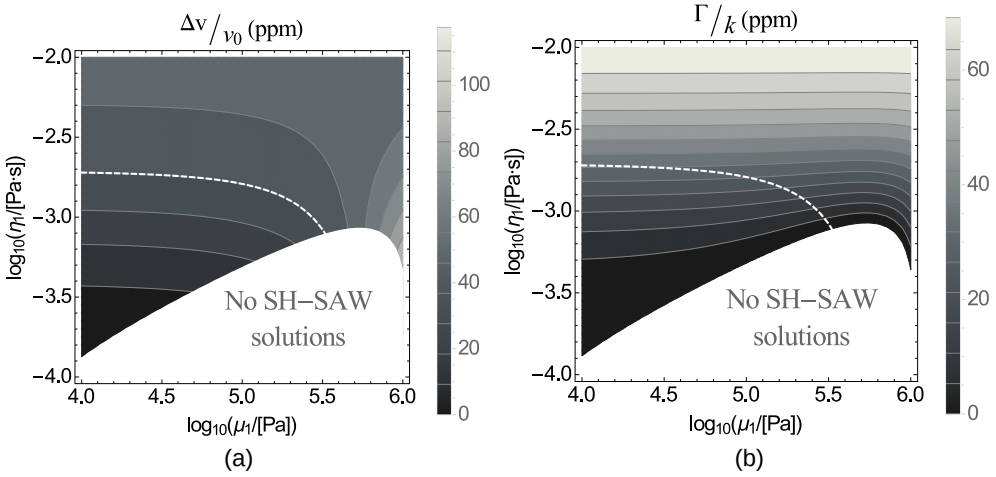

Fig. 11. Measurable characteristics for different film parameters with glycerol/water loading. The phase velocity shift (a) and scaled attenuation (b) at 100 MHz for a viscoelastic solid film ($h = 5$ nm) of varying parameters μ_1 and η_1, loaded by an 80% glycerol/water mixture, modeled as a viscoelastic fluid (scheme D, see Fig. 3). One contour line (dashed white line) in the velocity shift plot (a) is also plotted in the attenuation plot (b). Intersecting contour lines indicate that the two viscoelastic parameters should be distinguishable via measurements. The viscoelasticity of the film, influenced by viscoelastic coupling, destroys SH-SAWs in a region of parameter space (indicated).

4. Conclusions

We theoretically studied the interplay between the viscoelasticity of a film and that of a top fluid for SH-SAW sensors, modeled as a three-layer structure. This model, a soft film in a (viscoelastic) fluid, simulates the experimental conditions common for biosensors. From the dispersion equation, we derived analytical expressions (in the case of a thin film in a bulk fluid) for the phase velocity shift and the attenuation of SH-SAWs as a function of the storage and loss moduli, and the mass densities, of the two viscoelastic materials, Eqs. (20) and (21). Numerical calculations performed for selected examples of viscoelastic materials confirmed the analytical results, illustrating a so-called "missing mass effect" [42,18,31,19], a correction to the phase velocity shift and the attenuation coefficient due to viscoelastic coupling between the overlayers. The analytical expression derived in this work could prove useful in the interpretation of SH-SAW sensor data for soft films in liquid-phase environments, e.g., biosensor applications.

Glycerol/water mixtures of different glycerol concentrations were studied numerically using a combined Maxwell-Voigt scheme in Section 3.2, in order to clarify the role of viscoelastic fluid loading. Glycerol/water deserve special consideration since this mixture has been used for calibration of SH-SAW devices when measuring liposome or protein adsorption, and it has been shown that at higher concentrations these mixtures become increasingly Maxwellian [14].

For certain soft films, numerical calculations showed that the validity of SH-SAW solutions vanishes above a critical film thickness which depends on the viscoelastic parameters of both the film and the top fluid. The possibility of SH-SAWs being destroyed by viscoelastic coupling could be an important consideration in biosensing experiments.

Acknowledgments

We would like to thank the Swedish Research Council (VR) for funding and A. M. Eriksson and L. Y. Gorelik for useful discussions.

References

[1] M. Doi, S. Edwards, The theory of polymer dynamics, International Series of Monographs on Physics, Clarendon Press, 1986.
[2] D. Johannsmann, The Quartz Crystal Microbalance in Soft Matter Research: Fundamentals and Modeling, Soft and Biological Matter, Springer International Publishing, 2014.
[3] K. Länge, B.E. Rapp, M. Rapp, Surface acoustic wave biosensors: a review, Anal. Bioanal. Chem. 391 (5) (2008) 1509–1519, http://dx.doi.org/10.1007/s00216-008-1911-5.
[4] D.S. Ballantine, R.M. White, S.J. Martin, A.J. Ricco, E.T. Zellers, G.C. Frye, H. Wohltjen, Acoustic Wave Sensors: Theory, Design, and Physico-chemical Applications, Applications of Modern Acoustics, Academic Press, 1997.
[5] M. Saitakis, E. Gizeli, Acoustic sensors as a biophysical tool for probing cell attachment and cell/surface interactions, Cell. Mol. Life Sci. 69 (3) (2011) 357–371, http://dx.doi.org/10.1007/s00018-011-0854-8.
[6] E. Gizeli, Study of the sensitivity of the acoustic waveguide sensor, Anal. Chem. 72 (2000) 5967–5972.
[7] E. Gizeli, F. Bender, A. Rasmusson, K. Saha, F. Josse, R. Cernosek, Sensitivity of the acoustic waveguide biosensor to protein binding as a function of the waveguide properties, Biosens. Bioelectron. 18 (11) (2003) 71399–71406, http://dx.doi.org/10.1016/S0956-5663(03)00080-0.
[8] G. Hu, J. Xu, G.W. Auner, J. Smolinski, H. Ying, Viscosity response of shear horizontal surface acoustic wave on AlN/sapphire structure, Electron. Lett. 43 (18) (2007) 1006–1007.
[9] S. Lehtonen, V. Plessky, C. Hartmann, M. Salomaa, Unidirectional SAW transducer for GHz frequencies, IEEE Trans. Ultrason. 50 (2003) 817–820, http://dx.doi.org/10.1021/la801252t.
[10] E. Gizeli, N.J. Goddard, C.R. Lowe, A.C. Stevenson, A love plate biosensor utilising a polymer layer, Sensors Actuators B Chem. 6 (13) (1992) 131–137, http://dx.doi.org/10.1016/0925-4005(92)80044-X.
[11] G. Kovacs, G.W. Lubking, M.J. Vellekoop, A. Venema, Love waves for (bio)-chemical sensing in liquids, Ultrasonics Symposium, 1992, Proceedings., IEEE 1992, vol.1, 1992, pp. 281–285, http://dx.doi.org/10.1109/ULTSYM.1992.275995.
[12] E. Gizeli, C. Lowe, Biomolecular Sensors, CRC Press, 2003.
[13] K.A. Melzak, E. Gizeli, Love Wave Biosensors, John Wiley & Sons, Ltd, 2008 http://dx.doi.org/10.1002/9780470061565.hbb062.
[14] K. Saha, F. Bender, A. Rasmusson, E. Gizeli, Probing the viscoelasticity and mass of a surface-bound protein layer with an acoustic waveguide device, Langmuir 19 (4) (2003) 1304–1311, http://dx.doi.org/10.1021/la026806p.
[15] J. Andrä, A. Böhling, T.M.A. Gronewold, U. Schlecht, M. Perpeet, T. Gutsmann, Surface acoustic wave biosensor as a tool to study the interaction of antimicrobial peptides with phospholipid and lipopolysaccharide model membranes, Langmuir 24 (16) (2008) 9148–9153, http://dx.doi.org/10.1021/la801252t.
[16] N.-J. Cho, K.K. Kanazawa, J.S. Glenn, C.W. Frank, Employing two different quartz crystal microbalance models to study changes in viscoelastic behavior upon transformation of lipid vesicles to a bilayer on a gold surface, Anal. Chem. 79 (18) (2007) 7027–7035, http://dx.doi.org/10.1021/ac0709504.
[17] F. Martin, M.I. Newton, G. McHale, K.A. Melzak, E. Gizeli, Pulse mode shear horizontal-surface acoustic wave (SH-SAW) system for liquid based sensing applications, Biosens. Bioelectron. 19 (6) (2004) 627–632.
[18] M.V. Voinova, M. Rodahl, M. Jonson, B. Kasemo, Viscoelastic acoustic response of layered polymer films at fluid-solid interfaces: continuum mechanics approach, Phys. Scr. 59 (5) (1999) 391.
[19] M.V. Voinova, M. Jonson, B. Kasemo, Missing mass effect' in biosensor's QCM applications, Biosens. Bioelectron. 17 (10) (2002) 835–841.
[20] G. Sauerbrey, Verwendung von Schwingquarzen zur Wägung dünner Schichten und zur Mikrowägung, Z. Phys. 155 (1959) 206–212.
[21] K.K. Kanazawa, J.G. Gordon, The oscillation frequency of a quartz crystal resonator in contact with a liquid, Anal. Chim. Acta 175 (1985) 99–105.
[22] M.V. Voinova, E.S. Syrkin, Method of determining viscosity of liquid-crystalline Langmuir-Blodgett films, Crystallogr. Rep. 43 (5) (1998) 863–865.
[23] A.M. Kosevich, E.S. Syrkin, M.V. Voinova, Acoustical Imaging 21, Acoustic Sensors Using Langmuir-Blodgett Films, Springer, US, Boston, MA 1995, pp. 191–199.
[24] G. McHale, M.I. Newton, F. Martin, Theoretical mass sensitivity of love wave and layer guided acoustic plate mode sensors, J. Appl. Phys. 91 (12) (2002) 9701–9710, http://dx.doi.org/10.1063/1.1477603.

[25] C. McMullan, E. Gizeli, H. Mehta, C.R. Lowe, Modelling of the mass sensitivity of the love wave device in the presence of a viscous liquid, J. Phys. D. Appl. Phys. 33 (23) (2000) 3053.
[26] M.V. Voinova, M. Jonson, B. Kasemo, Dynamics of viscous amphiphilic films supported by elastic solid substrates, J. Phys. Condens. Matter 9 (37) (1997) 7799.
[27] J. Liu, A simple and accurate model for love wave based sensors: dispersion equation and mass sensitivity, AIP Adv. 4 (7) (2014) 077102, http://dx.doi.org/10.1063/1.4886773.
[28] H. Oh, W. Wang, K. Lee, S. Yang, Sensitivity evaluation of a love wave sensor with multilayer structure for biochemical application, Proc. SPIE 7207 (2009) http://dx.doi.org/10.1117/12.809982 (72070R–72070R–8).
[29] G. McHale, M.I. Newton, F. Martin, Theoretical mass, liquid, and polymer sensitivity of acoustic wave sensors with viscoelastic guiding layers, J. Appl. Phys. 93 (1) (2003) 675–690, http://dx.doi.org/10.1063/1.1524309.
[30] L.D. Landau, E.M. Lifshitz, Theory of Elasticity, Butterworth-Heinemann, Oxford, 2008.
[31] M.V. Voinova, Modelling of the response of acoustic piezoelectric resonators in biosensor applications - part 1: the general theoretical analysis, J. Sens. Sens. Syst. 4 (2015) 137–142.
[32] E. Calderon, M. Gauthier, F. Decremps, G. Hamel, G. Syfosse, A. Polian, Complete determination of the elastic moduli of Î ± -quartz under hydrostatic pressure up to 1 GPa: an ultrasonic study, J. Phys. Condens. Matter 19 (43) (2007) 436228.
[33] R. Christensen, Theory of Viscoelasticity, Civil, Mechanical and Other Engineering Series, Dover Publications, 2003.
[34] http://www.makeitfrom.com/material-properties/Polymethylmethacrylate-PMMA-Acrylic, accessed 2016-02-24.
[35] J. A. Phelps, S. Morisse, M. HindiÃ©, M.-C. Degat, E. Pauthe, P. R. V. Tassel, Nanofilm biomaterials: localized cross-linking to optimize mechanical rigidity and bioactivity, Langmuir 27 (3) (2011) 1123–1130, http://dx.doi.org/10.1021/la104156c. (pMID: 21182246)
[36] K. Mitsakakis, A. Tsortos, J. Kondoh, E. Gizeli, Parametric study of SH-SAW device response to various types of surface perturbations, Sensors Actuators B Chem. 138 (2) (2009) 408–416, http://dx.doi.org/10.1016/j.snb.2009.02.050.
[37] J. Liu, A theoretical study on love wave sensors in a structure with multiple viscoelastic layers on a piezoelectric substrate, Smart Mater. Struct. 23 (7) (2014) 075015.
[38] J. Liu, L. Wang, Y. Lu, S. He, Properties of love waves in a piezoelectric layered structure with a viscoelastic guiding layer, Smart Mater. Struct. 22 (12) (2013) 125034.
[39] J. Liu, L. Wang, S. He, On the fundamental mode love wave in devices incorporating thick viscoelastic layers, Chin. Phys. Lett. 32 (06) (2015) 064301.
[40] G. McHale, M.I. Newton, F. Martin, Layer guided shear horizontally polarized acoustic plate modes, J. Appl. Phys. 91 (9) (2002) 5735–5744.
[41] G. McHale, M.I. Newton, F. Martin, E. Gizeli, K.A. Melzak, Resonant conditions for love wave guiding layer thickness, Appl. Phys. Lett. 79 (21) (2001) 3542–3543, http://dx.doi.org/10.1063/1.1420776.
[42] D. Johannsmann, Viscoelastic analysis of organic thin films on quartz resonators, Macromol. Chem. Phys. 200 (1999) 501–516.